Single-pot synthesis of Ti-SBA-15-NiMo hydrodesulfurization catalysts: Role of calcination temperature on dispersion and activity

Saheed A. Ganiyu [a,b], Khalid Alhooshani [a,*], Syed Ahmed Ali [c]

[a] Department of Chemistry, King Fahd University of Petroleum & Minerals, Dhahran 31261, Saudi Arabia
[b] Center of Research Excellence in Nanotechnology, King Fahd University of Petroleum & Minerals, Dhahran 31261, Saudi Arabia
[c] Center of Research Excellence in Petroleum Refining & Petrochemicals, King Fahd University of Petroleum & Minerals, Dhahran 31261, Saudi Arabia

ARTICLE INFO

ABSTRACT

A novel approach was systematically investigated for developing single-pot (SP) NiMo-supported Ti-SBA-15 catalysts for hydrodesulfurization (HDS). The technical challenge associated with the SP approach is the formation of crystalline $NiMoO_4$, and this was avoided by reducing the calcination temperature of the oxide catalyst from 550 °C to 300 °C to form a highly dispersed and efficient HDS catalyst. The dispersion, textural properties, surface acidity, oxide reducibility, surface chemical and elemental compositions of developed catalysts were measured by XRD, Raman spectroscopy, N_2-physisorption, and temperature-programmed techniques (TPR and TPD), X-ray photoelectron spectroscopy (XPS) and inductively coupled plasma (ICP). Scanning electron microscopy (SEM), and high resolution transmission electron microscopy (HRTEM) were employed as additional characterization methods to investigate the catalysts' morphology and microstructure. Catalyst performance was evaluated in a batch autoclave reactor using a simulated feed containing 2500 parts per million sulfur (ppm-S) (dibenzothiophene, DBT) in dodecane. The catalyst prepared by the SP approach and calcined at a lower temperature (300 °C) showed significantly improved HDS activity and direct desulfurization selectivity compared to the catalyst prepared by the conventional impregnation approach. An increase in the calcination temperature to 550 °C, however, resulted in a decrease in the HDS activity of the catalysts prepared by both methods. The dispersion, surface acidity, and textural properties of the catalysts prepared using the SP method combine to improve the catalytic efficiency. The use of a complexing agent to aid the dispersion of the active phase was unnecessary when the SP method was used for catalyst preparation.

© 2016 Elsevier B.V. All rights reserved.

1. Introduction

Stringent environmentally driven regulations limiting the sulfur content in transportation fuels and the development of sulfur-free fuel cells continue to challenge researchers to develop highly active and stable hydrodesulfurization (HDS) catalysts. Several research efforts toward improving HDS catalysis have been reported, such as changing or modifying the type or nature of the support, the active metals, the synthesis routes, and the use of organic or inorganic additives [1,2].

γ-Al_2O_3 has been the most widely used support for hydrotreating catalysts, but it interacts strongly with the active phase metal (MoO_3) in a monolayered tetrahedral coordination. This interaction inhibits active phase reduction, which in turn decreases catalytic activity compared to octahedral Mo [3]. Mesoporous supports, such as silica, novel zeolites, carbon, titania, and mixed metal oxides, are reported to provide significant improvements compared to γ-Al_2O_3 [4–9].

SBA-15 is one of the most studied mesoporous silica materials due to its high surface: volume ratio, high pore size, highly ordered 2D hexagonal structure, good mechanical strength, and thick pore wall, which is responsible for hydrothermal stability among other silicas. SBA-15 possesses a combination of micropores (0.5–3.0 nm) and mesopores (4–14 nm) in a uniform hexagonal tunable pore structure [10]. Recently, the use of SBA-15 as an HDS support has tremendously increased because of its catalytic properties; however, poor dispersion of the active phase(s) hindered its full catalytic potential.

To overcome this limitation, different modification approaches, such as the incorporation of transition metals, the addition of chelating agents, and the use of additives, have been reported. For example, chelating agents, such as nitriloacetic acid (NTA),

* Corresponding author.
E-mail address: hooshani@kfupm.edu.sa (K. Alhooshani).

ethylenediaminetetraacetic acid (EDTA), cyclohexanediaminetetraacetic acid (CyDTA), and citric acid (CA), have been shown to improve the performance of SBA-based HDS catalysts [11–14]. The addition of chelating agents renders β-CoMoO$_4$ or NiMoO$_4$ soluble by increasing the dispersion of Co or Mo without blocking active sites [15]. Moreover, the incorporation of heteroatoms (Ti, Zr, and Al) and organic functional groups, either by a direct or post-synthesis approach, have reportedly improved the stability and activity of SBA-15 HDS catalysts [16]. The heteroatoms are Lewis acids and can improve the dispersion of the active phase by increasing the metal-support interaction (MSI) from low to moderate.

Badoga et al. [17] studied the combined effect of heteroatoms and complexing agents in the direct synthesis of M-SBA-15 (Ti, Zr, and Al) followed by the dispersion of the active phase with the aid of EDTA via the impregnation method. The HDS activities for NiMo/Ti-SBA-15 and NiMo/Ti-SBA-15/2EDTA were improved by 12% and 18%, respectively, as a result of the increased surface acidity and MSI.

Pena et al. [18] reported the significance of EDTA and CA in enhancing the HDS catalytic activity (91.6% after 8 h of reaction) of DBT. They claimed that the use of chelating agents avoided the formation of a crystalline (CoMoO$_4$) phase and resulted in better dispersion of MoO$_3$, as confirmed by XRD and HRTEM. Valencia and Klimova [19] studied the effect of citric acid (CA) loading on the sulfided NiMo supported on SBA-15 for HDS of DBT. Their investigation revealed that increase in the amount of CA resulted in better dispersion of active metals (Ni and Mo) as confirmed by XRD and DRS, and consequently on the selectivity of the catalysts towards direct desulfurization (DDS) route. In addition, they showed that all catalysts prepared with CA have higher activity than without CA, but the increase in the amount of CA beyond (2.7) decreases the activity. By establishing the correlation between the concentration of Mo and Ni on the edges of sulfide particles and the catalytic HDS activities, Gutieírrez et al. [20] highlighted the influence of the nature of the support on the dispersion of non-promoted catalysts and the degree of Ni decoration on the edges of the Ni-Mo-S phase.

The use of additives such as fluorine and phosphorus has been reported, but non-noble metal-based HDS catalysts, such as transition metal phosphides with SBA-15 and molybdenum carbide-SBA-15, have not been extensively studied, despite their excellent HDS activities [21,22]. However, supported noble metals are susceptible to sulfur poisoning due to the strong interaction with H$_2$S, which limits their use in hydrotreating processes [23]. The synthesis routes and conditions of the support, which can improve textural properties, provide alternative ways to improve the catalytic activity of HDS catalysts.

Despite research efforts to improve the catalytic activities of SBA-15, including the deposition of active metals via equilibrium adsorption, sequential and co-impregnation, mechanical mixing, sol-gel approach, and grafting, there are no extensive literature reports on the single-pot synthesis of Ti-SBA-15-NiMo with or without a complexing agent in the same mixture for the HDS reaction. Therefore, the present work adopts a facile approach in the development of an HDS catalyst via the single-pot (SP) synthesis of a modified mesoporous SBA-15 support and active phase(s) with or without a complexing agent by the hydrothermal (HT) method. The SP approach presents new, simple, and easy steps in catalyst design and preparation, which allows low-cost catalyst design and active phase incorporation within the mesoporous framework. In addition, effect of calcination temperature was studied as a function of catalysts dispersion and activity, and catalysts were characterized by X-ray diffraction (XRD), N$_2$-physisorption, Raman spectroscopy, Fourier transform Infra-red (FTIR), temperature programmed analysis by desorption and reduction (TPD and TPR), scanning and transmission electron microscope (SEM and TEM), and X-ray photoelectron spectroscopy (XPS).

2. Experimental section

2.1. Materials

Tetraethylorthosilicate (TEOS) (C$_2$H$_5$O)$_4$Si as the silica source, pluronic P123 PEO$_{20}$-PPO$_{70}$-PEO$_{20}$ triblock copolymer as the structural directing agent, nickel nitrate hexahydrate (99%) as the nickel precursor, titanium isopropoxide (97%) as the titanium source, citric acid (99.7%), dibenzothiophene (DBT) (98%), and dodecane were purchased from Sigma-Aldrich. Ammonium molybdate (VI) tetrahydrate (99%) was obtained from ACROS organics. High-purity deionized water (18 μS/cm) was produced in-house using *Thermo Scientific Barnstead NANOPURE* after distillation with a *Labstrong FiSTREEM*^{TM} *II 2S Glass Still* distiller.

2.2. Synthesis of SBA-15 and titanium-modified SBA-15 support

Mesoporous SBA-15 and Ti-SBA-15 (Si/Ti = 10) were prepared using procedures described by Zhao et al. [24] via the hydrothermal (HT) synthesis method. Typically, SBA-15 was prepared from a reaction mixture of 60 g of 2 M HCl, 4.16 g of TEOS, 2 g of P123, and 15 g of deionized water stirred at 500 rpm for 24 h at 40 °C. The mixture was transferred into a Teflon-lined autoclave and then heated for 24 h according to the HT method at 100 °C. The synthesized SBA-15 was calcined at 550 °C for 6 h (ramp rate of 10 °C/min) for template removal. For Ti-SBA-15, the same procedure was followed but with the incorporation of an equivalent amount of titanium isopropoxide to the mixture after stirring the TEOS-surfactant mixture for 90 min.

2.3. Single-pot (SP) synthesis of Ti-SBA-15-NiMo catalyst

The single-pot (SP) synthesis of HDS catalyst was accomplished by modifying the sol-gel preparation route for SBA-15, as illustrated in Fig. 1. This method involves the addition of approximately 4.16 g TEOS to a mixture containing a well-dispersed 2 g (P123) in 60 g of 2 M HCl and 15 g of deionized water, which was stirred for 30 min. The titanium precursor in a 10:1 (Si:Ti) molar ratio was added before the hydrolysis of TEOS and stirred continuously for 20 h. A mixture of the Mo and Ni (13 wt.% and 3 wt.%, respectively) precursors without or with citric acid (CA:Mo ratio of (1:1)) [25], which were previously mixed at room temperature (RT) for 1 h, was added to the synthesis pot and stirred vigorously for 3 h at RT without pH adjustment (pH < 1). The mixture was transferred to a Teflon-lined autoclave for hydrothermal (HT) synthesis at 100 °C for 24 h. The solid product was then centrifuged and washed with deionized water before drying at 100 °C for 12 h and subjected to final calcination at either 300 °C or 550 °C for 6 h in a muffle furnace. The heating rate during calcination was maintained at 10 °C/min.

2.4. Impregnation of NiMo active phase on the support

The impregnation of NiMo active phase on the support was performed by the excess wet solution method in deionized water. The procedure involves stirring equivalent amounts of nickel and molybdenum precursors (to obtain 3 wt.% and 13 wt.% of metal, respectively, in the catalyst) at room temperature for 3 h without or with citric acid (CA:Mo ratio of 1:1), followed by the addition of 1 g Ti-SBA-15 to the mixture without pH adjustment (pH 4–5). This mixture was stirred for 2 h and then dried by slow evaporation at 60–70 °C. Prior to final calcination at 300 or 550 °C, the catalyst was dried at 100 °C for 12 h.
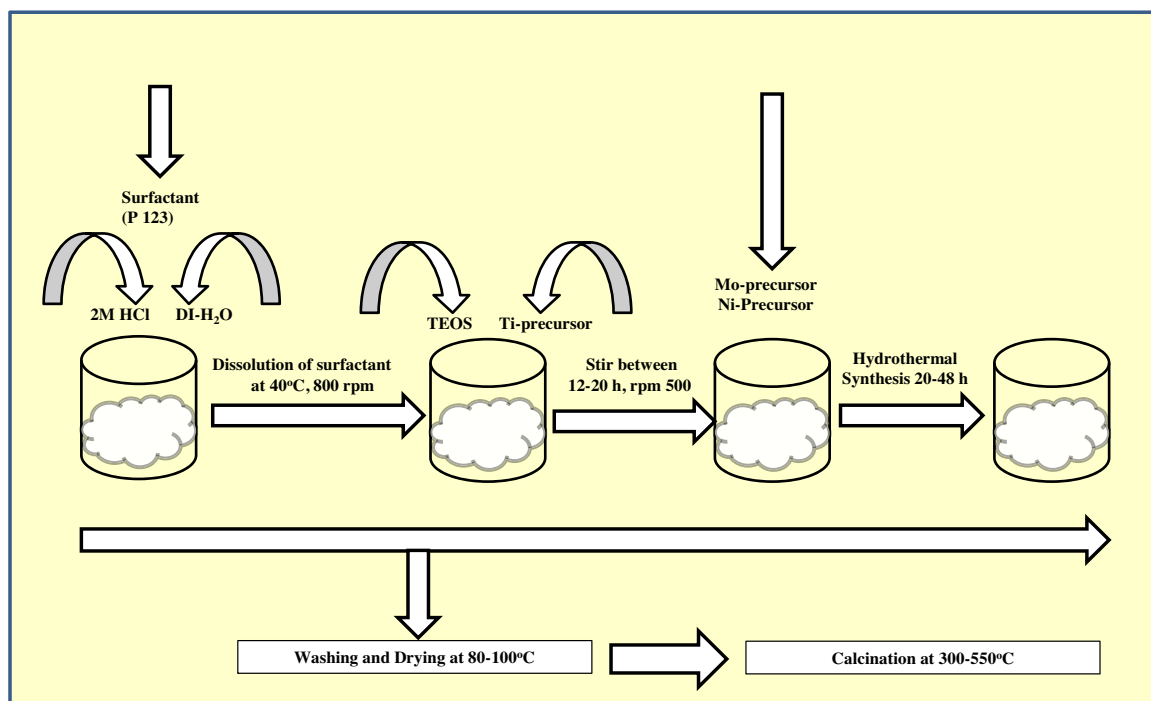
Fig. 1. Schematic Representation of Single-Pot (SP) Synthesis of NiMo Supported on Metal-Modified SBA-15 Catalysts.

Table 1
Description of Supports and Catalysts.

Sample Code	Description	Catalyst Preparation Method	Calcination Temperature (°C)
SBA-15	Template-free SBA-15	–	550
Ti-SBA-15	Titanium-modified SBA-15	–	550
TSMN-Imp300	NiMo/Ti-SBA-15	Impregnation	300
TSMN-Imp550	NiMo/Ti-SBA-15	Impregnation	550
TSMN-SP300	NiMo-Ti-SBA-15	Single-Pot	300
TSMN-SP550	NiMo-Ti-SBA-15	Single-Pot	550
TSMN(CA)-Imp300	NiMo/Ti-SBA-15 with citric acid	Impregnation	300
TSMN(CA)-Imp550	NiMo/Ti-SBA-15 with citric acid	Impregnation	550
TSMN(CA)-SP300	NiMo-Ti-SBA-15 with citric acid	Single-Pot	300
TSMN(CA)-SP550	NiMo-Ti-SBA-15 with citric acid	Single-Pot	550

Table 1 lists the supports and catalysts prepared and investigated in this study along with their codes and descriptions. The Ti-SBA-15-NiMo catalysts prepared by the single-pot method with and without a complexing agent are denoted as TSMN(CA)-SP(x) and TSMN-SP(x), respectively, where x represents the calcination temperature. The Ti-SBA-15/NiMo catalysts prepared by the impregnation method with and without a complexing agent are denoted as TSMN(CA)-Imp(x) and TSMN-Imp(x), respectively, where x represents the calcination temperature.

2.5. Characterization of supports and catalysts

2.5.1. Textural properties
The BET surface area, pore size, and pore volumes were measured on a Micromeritics ASAP 2020 using N_2 adsorption-desorption at −196 °C. Prior to measurement, the samples were degassed at 250 °C for 3 h to remove impurities or moisture. The Brunauer, Emmett, and Teller (BET) method was used to calculate the surface area, and the adsorption part of Barrett, Joyner, and Halenda (BJH) method was used to calculate the pore size distribution and pore volume.

2.5.2. Thermogravimetric analysis
Thermal analysis of the prepared catalysts was performed on an SDTQ600 TGA in high-purity zero air. The furnace temperature was increased from 30 °C to 1000 °C at a rate of 10 °C/min, whereas the cooling rate was 30 °C/min.

2.5.3. X-ray diffraction
X-ray diffraction (XRD) at a wide angle using Cu anode (9 kV) at Kα = 1.5405 (Rigaku miniflex-bench top X-ray powder) was used to determine the crystallinity of the prepared catalysts. The samples were scanned between 20° and 80° at 3°/min.

2.5.4. Raman spectroscopy
A Raman spectroscope (HORIBA, iHR320 with CCD detector) with a laser wavelength of 532 nm (300 mW, green laser) was used to characterize the MoO_3 and TiO_2 phases.

2.5.5. Fourier transformation infrared (FTIR) spectroscopy
FTIR was used to identify the functional groups present in the developed supports and catalysts. The (IR) absorption spectra of SBA-15, Ti-SBA-15, and NiMo-supported catalysts were recorded on a Thermo Scientific Nicolet 6700 FT-IR spectrometer with a scanning range of 400–4000 cm^{-1}. The samples for FTIR analysis were

Table 2
Textural Properties of Supports and Catalysts.

Sample Code	BET Surface Area (m²/g)	Microporous Surface Area (m²/g)	External Surface Area (m²/g)	Microporous Pore Volume (cm³/g)	Total Pore Volume (cm³/g)	Average Pore Size (nm)
SBA-15	643	47	595	0.023	1.25	7.9
Ti-SBA-15	679	81	596	0.040	1.39	8.3
TSMN-Imp300	146	21	125	0.011	0.16	6.1
TSMN-Imp550	145	21	125	0.010	0.33	8.8
TSMN-SP300	403	30	374	0.014	0.66	6.5
TSMN-SP550	260	17	244	0.008	0.45	6.6
TSMN(CA)-Imp300	160	14	146	0.007	0.19	5.5
TSMN(CA)-Imp550	103	11	92	0.005	0.21	7.6
TSMN(CA)-SP300	352	28	324	0.013	0.51	6.3
TSMN(CA)-SP550	155	18	137	0.009	0.77	6.9

prepared using KBr powder mixed with the support/catalyst in a ratio of 100:1 to form pellet-like translucent discs.

2.5.6. Temperature-programmed desorption of ammonia (NH$_3$-TPD)

Surface acidity measurement was conducted on a Micromeritics Chemisorb 2750 (pulse chemisorption system) using 10 wt.% NH$_3$ by temperature-programmed desorption (TPD). Approximately 100 mg of non-sulfided catalyst was loaded into a quartz tube and covered with quartz. The sample was purged with high purity helium at 600 °C and held for 30 min before being cooled to 100 °C. The probe molecule (NH$_3$) was adsorbed on the sample at 100 °C for 30 min, which was followed by helium purging for 60 min to remove any physisorbed ammonia. NH$_3$ desorption was accomplished by heating the furnace at 10 °C/min to 800 °C, and the data were recorded with a thermal conductivity detector (TCD).

2.5.7. Temperature-programmed reduction by hydrogen (TPR-H$_2$)

The reducibility potential of metal oxides supported on Ti-SBA-15 was determined by temperature-programmed reduction with hydrogen as the probe molecule using a Micromeritics (Autochem II-2920) chemisorption analyzer. Approximately 50 mg of the prepared catalyst previously calcined at 300 °C or 550 °C was pre-treated for one hour in high-purity helium at 500 °C and then cooled to ambient temperature before being heated to 1000 °C at 10 °C/min under a steady flow (20 ml/min) of 10% H$_2$ in helium. The consumption of H$_2$ at the reducible temperature(s) was recorded on a thermal conductivity detector (TCD).

2.5.8. Field emission scanning electron microscopy (FE-SEM)

The TESCAN LYRA 3 unit was used to examine the morphology of SBA-15 and modified SBA-15-NiMo catalysts using secondary electron (SE) and backscattered electron (BSE) modes at an accelerating voltage of 30 kV. The unit was equipped with an energy-dispersive X-ray spectrometer (EDS, Oxford, Inc.) detector for elemental analysis.

2.5.9. Transmission electron microscopy (TEM)

Microstructural and morphological analysis of sulfided NiMo HDS catalysts was performed on FEI Titan 300, high resolution transmission electron microscope (HRTEM), operated at 120 kV. The sample preparation was performed by dispersing sulfided catalysts powder in ethanol until total dissolution, which was followed by deposition of an air-dried sample on a carbon coated grid for TEM analysis.

2.5.10. X-ray photoelectron spectroscopy (XPS)

The bonding state and chemical composition of sulfided HDS catalysts were determined by X-ray photoelectron spectroscope (PHI 5000 Versa Probe II, ULVAC-PHI Inc.). The sample preparation

was done by making a few centimeter pelletized disc and subjected to high vacuum before XPS analysis.

2.5.11. Elemental analysis by ICP-OES

The elemental composition of the bulk catalysts for Si, Ti, Mo and Ni were determined by inductively coupled plasma (ICP) attached with optical emission spectrometer (Ultima 2, Horiba Scientific). Typical sample preparation procedure involves fusing a 50 mg of catalyst sample with 350 mg of lithium metaborate in a muffle furnace at 1000 °C for 20 min. The fused product was dissolved in 10 ml of 10% HNO$_3$ and diluted with deionized water to make a total volume of 50 ml. The solution thus obtained was analyzed by ICP-OES.

2.6. Presulfiding and performance evaluation of catalysts

Samples of prepared catalysts were pelletized, crushed, and sieved into 300–500 μm sizes. Each sample was reduced under a flow of 5% H$_2$/He (60 ml/min) at 400 °C (ramp rate of 10 °C/min) for 2 h to convert Ni and Mo to metallic forms. Presulfidation was performed using a solution containing 2 wt.% CS$_2$ in a quartz tube at 350 °C overnight.

The HDS performance of prepared catalysts was evaluated in a high-pressure batch reactor (model: Parr 4576B) at 350 °C under 5 MPa of H$_2$ pressure and constant 300 rpm stirring. Approximately 0.25 g of catalyst was added to 100 ml of the simulated feed containing DBT (2500 ppm-S) in dodecane. Each test was conducted for 4 h after the target process conditions were achieved. Product samples were collected every hour during this period.

The sulfur content in the feed and products was quantified using a gas chromatography sulfur chemiluminiscence detector (GC-SCD), and product identification was achieved with gas chromatography mass spectrometry (GC–MS). Hydrocarbon analysis was performed with a gas chromatography flame ionization detector (GC-FID).

3. Results and discussion

3.1. Characterization results

3.1.1. Textural properties

The textural properties of synthesized supports (SBA-15 and Ti-modified SBA-15) and NiMo catalysts without sulfidation are presented in Table 2, and the adsorption-desorption isotherms are presented in Fig. 2. The parent SBA-15 exhibits a high specific surface area (643 m²/g) and large pore volume (1.25 cm³/g), with an average pore diameter of 7.9 nm. It exhibits a type-IV isotherm showing an H1 hysteresis loop, which is a typical characteristic of mesoporous SBA-15 silica according to IUPAC [10]. Notably, the incorporation of titanium into SBA-15 improves its textural properties (for instance, the surface area is increased to 679 m²/g).
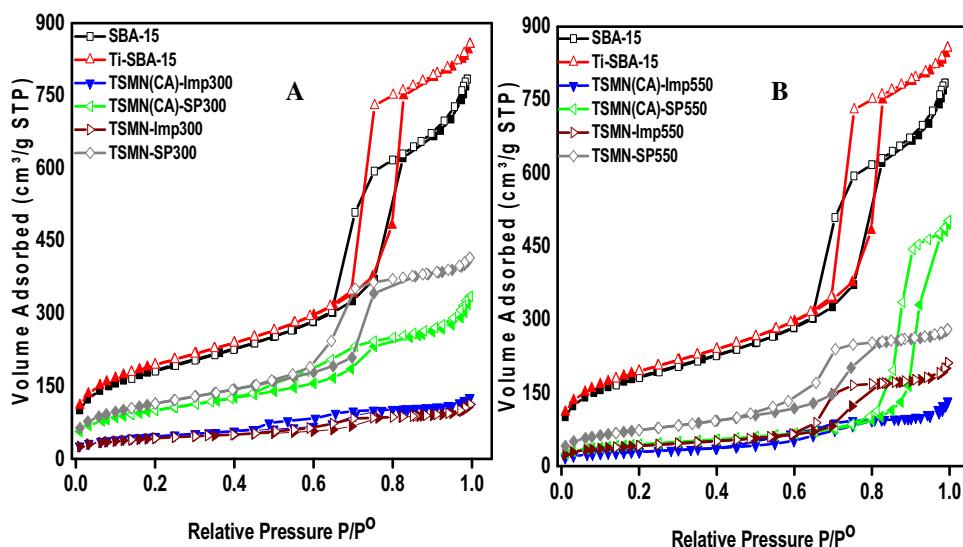
Fig. 2. Nitrogen Adsorption-Desorption Isotherms of Catalysts Calcined at (A) 300 °C and (B) 550 °C.

The introduction of Ni and Mo onto Ti-SBA-15 either by impregnation or through the single-pot approach, however, reduces the pore size due to surface and void blockage. Nitrogen adsorption and desorption isotherms (Fig. 2) provide the evidence of particles plugged within the support matrix. The catalysts prepared by the SP approach exhibit higher surface areas than those prepared by the impregnation method. The relative preservation of textural properties by the SP approach is likely due to the ability of the active metal-oxides to be embedded into the support matrix without total surface coverage. It can thus be expected that the SP approach will create a highly dispersed active phase for efficient catalytic performance.

3.1.2. Thermogravimetric analysis

The thermal stability of the synthesized catalysts was evaluated by thermogravimetric analysis (TGA) in which weight loss or phase change is observed upon heating the catalyst samples to 1000 °C. SBA-15 has been reported to possess higher hydrothermal stability due to the thick microporous silica pore wall (3–6 nm) compared to MCM-41, MCM-48, and HMS [26].

TGA of the TSMN catalyst sample without calcination reveals that the major weight loss occurs below 300 °C due to the loss of surfactants and adsorbed water, as shown in Fig. 3. When the catalysts that were calcined at different temperatures between 300 °C and 550 °C were subjected to TGA, the results show similar trends in the thermal stability up to 700 °C, as shown in Fig. 3. Therefore, a calcination temperature of 300 °C is sufficient to remove surfactants and adsorbed water from the catalysts synthesized by the SP method with or without complexing agent (See Fig. SI-1).

3.1.3. X-ray diffraction

X-ray powder diffraction (XRD) analysis enabled the determination of the crystallinity and different phases of the synthesized supports (SBA-15 and Ti-SBA-15) and the NiMo catalysts supported on Ti-SBA-15. The structure of SBA-15 in low-angle XRD exhibits three characteristic diffraction peaks of silica and, these peaks are associated with p6 mm ordered hexagonal symmetry, indexed as (100), (110), and (200) [27]. Additionally, as shown in Fig. 4 from wide-angle XRD, the MoO_3 characteristic peaks are identified at different peak positions. The major peaks at 2-theta of 13, 23.42, 26, 27.52, and 39° are due to the orthorhombic MoO_3 crystalline phase [28], whereas peaks at 2-theta of 26, 39, and 67, which mostly coincide with and are overlaid by MoO_3, indicate TiO_2 anatase [29].
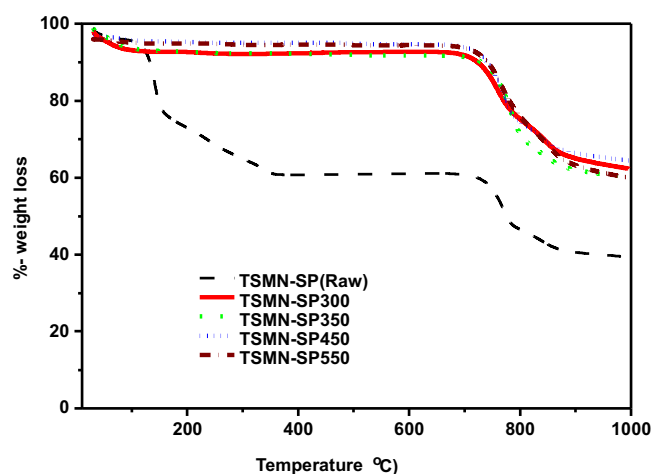

Fig. 3. Thermogravimetric Analysis of Catalysts Prepared by the SP Method and Calcined at Different Temperatures.

The diffraction peak associated with nickel could not be identified due to concentration limitations in XRD for the metal oxides. The molybdena present in all catalysts subjected to high temperature calcination can be indexed to orthorhombic MoO_3 (JCPDS card no. 05-0508) with the space group Pbnm of octahedral form. As shown in Fig. 4B, the catalyst prepared by impregnation with a complexing agent (TSMN(CA)-Imp550) at a higher calcination temperature shows exceptional characteristics of MoO_3 reflections unlike others, due to high intensity of the peak centered at $2\Theta = 26°$. In general, the catalysts calcined at 300 °C show better dispersion on the support with broadened peaks and low intensities of the (020), (040), and (060) phases corresponding to MoO_3 particles, which signifies the presence of small crystallites [30].

3.1.4. Raman spectroscopy

Raman spectroscopy is a non-destructive method for characterizing the dispersion of active metal on the support [31]. Molybdenum oxide and titanium oxide phases for the HDS NiMo catalysts were examined using a laser Raman spectroscope, with the crystalline molybdena existing either in the tetrahedral (tet) or octahedral (oct) form [32]. For pure MoO_3 crystallites, the peaks at 819 and 665 cm^{-1} are characteristic of the Mo—O—Mo bridge
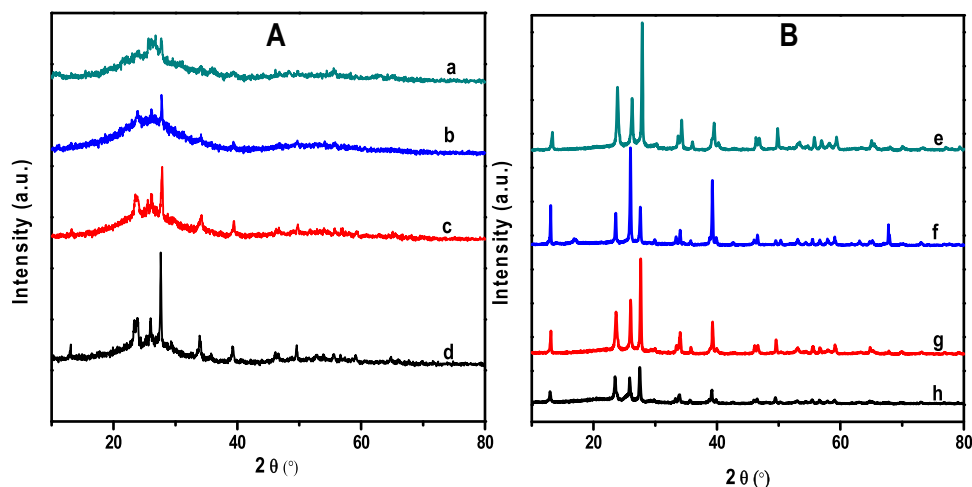
Fig. 4. X-ray Diffraction Analysis of HDS Catalysts. [(A) (a) TSMN-Imp300, (b) TSMN(CA)-Imp300, (c) TSMN-SP300, (d) TSMN(CA)-SP300], and [(B) (e) TSMN-Imp550, (f) TSMN(CA)-Imp550, (g) TSMN-SP550, (h) TSMN(CA)-SP550].
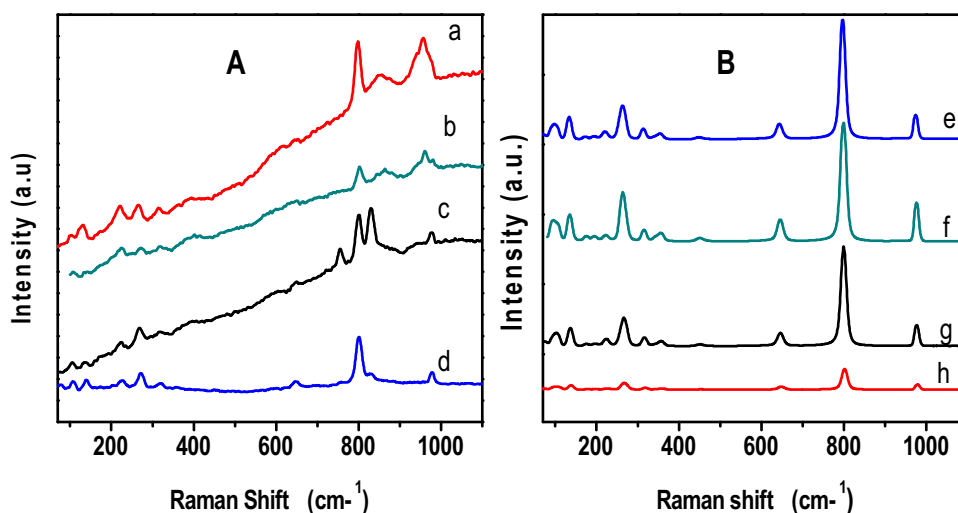

Fig. 5. Raman Analysis of HDS Catalysts. [(A) (a) TSMN-Imp300, (b) TSMN(CA)-Imp300, (c) TSMN-SP300, (d) TSMN(CA)-SP300], and [(B) (e) TSMN-Imp550, (f) TSMN(CA)-Imp550, (g) TSMN-SP550, (h) TSMN(CA)-SP550].

stretching mode, whereas symmetric stretching of the Mo=O terminal oxygen is observed at 994 cm^{-1} [33,34]. The bands at 336 and 375 cm^{-1} could be assigned to the bending and deformation modes of vibrations of O=Mo=O and O—Mo—O, and the Mo=O wagging mode of vibration is observed at 290–280 cm^{-1} [35,36]. As shown in Fig. 5, the characteristic MoO$_3$ peaks are observed in all NiMo catalysts prepared at the higher calcination temperature (550 °C), with differences in their peak intensities and positions due to different degrees of interaction with the supports (related to the degree of crystallinity and/or dispersion). The dominant molybdena species due to the interaction on SBA-15 may exist in the form of tetrahedral (Si—O—)$_2$Mo(=O)$_2$ di-oxo species, due to the presence of bands at 970 and 355 cm^{-1} [37]. However, good dispersion is achieved for the NiMo oxide catalysts subjected to a lower calcination temperature, as evidenced by the presence of amorphous peaks at 950 cm^{-1} [38].

Notably, Ti-SBA-15 synthesized by the direct approach before the addition of NiMo for the HDS oxide catalysts exhibits five peaks corresponding to the anatase phase of titania. Peak analysis reveals that the stretching (E$_g$) mode of vibrations in O—Ti—O is observed at 144, 197, and 630 cm^{-1}, whereas the symmetric (B$_{1g}$) and asymmetric (A$_{1g}$) bending vibrations are at 395 and 520 cm^{-1},

respectively [39]. However, upon the introduction of Mo into the matrix support, all modes of vibrations assigned to titania (anatase) become unobservable, perhaps due to the dominance of Mo (see Supporting Fig. SI-2). Therefore, the observed peaks shown in Fig. 5 are assigned only to MoO$_x$ phases of either crystalline SP or impregnation HDS catalysts.

3.1.5. FTIR spectroscopy

FTIR spectroscopy was employed to gain insight into the functional groups of SBA-15, Ti-SBA-15, and NiMo-modified Ti-SBA-15 catalysts. As shown in Fig. 6, SBA-15 shows a strong intensity band at approximately 1218 cm^{-1}, corresponding to the asymmetric stretching modes of Si—O—Si, along with a broad absorption band at 1628 cm^{-1}, which is characteristic of the —OH stretching of an absorbed water molecule [40]. The band at 3500 cm^{-1} can be associated with the silanol end group (Si—OH) and Si$_3$—O—Ti—OH due to Brønsted acid sites. The incorporation of Ti into the SBA-15 mesoporous silica network results in bands at 800 and 950 cm^{-1} due to the Ti—O symmetric stretching mode and Ti—O—Si bending modes, respectively [17]. For NiMo-supported SBA-15, the Mo—O—Mo stretching mode is observed at approximately 620 and 850 cm^{-1}, and the band at 797 cm^{-1} corresponds to the presence of
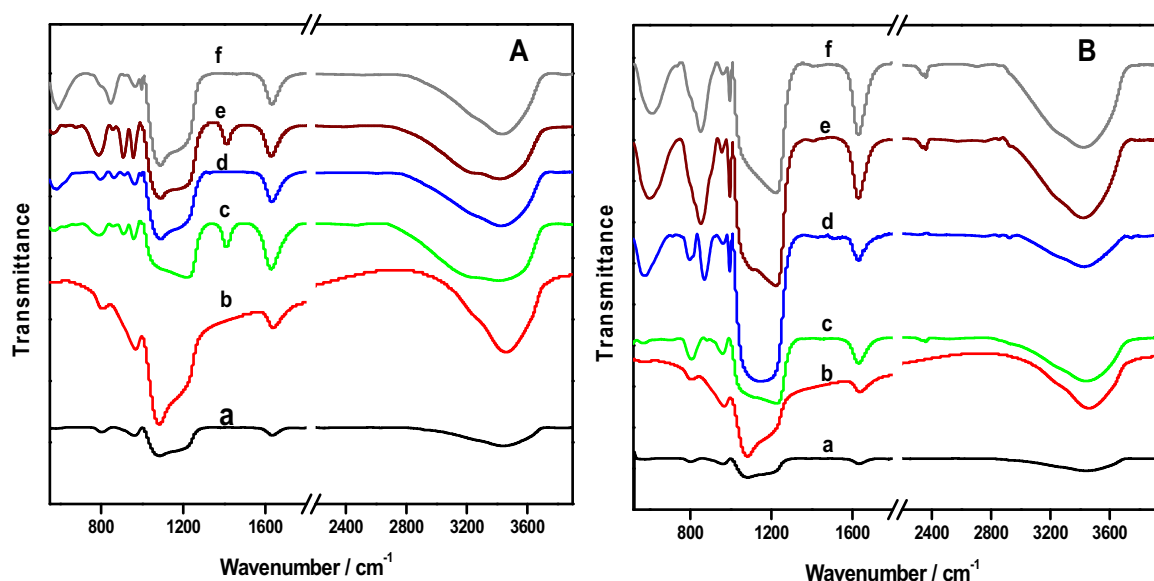
Fig. 6. FTIR Results of Supports and Catalysts. [A] (a) SBA-15; (b) Ti-SBA-15; (c) TSMN(CA)-Imp300; (d) TSMN(CA)-SP300; (e) TSMN-Imp300; (f) TSMN-SP300, and [B] (a) SBA-15; (b) Ti-SBA-15; (c) TSMN(CA)-Imp550; (d) TSMN(CA)-SP550; (e) TSMN-Imp550; (f) TSMN-SP550..

Table 3
TPD and TPR Results of Catalysts (in the Oxide Form).

Catalysts			TPR: H_2-consumption	
	Peak Temperature(s) (°C)	Amount (mmol/g)	Peak Temperature(s) (°C)	Amount (mmol/g)
TSMN-Imp300	206	0.158	640.57	29.49
TSMN-Imp550	202	0.085	720, 1000	66.43
TSMN-SP300	195	0.198	571, 950	44.22
TSMN-SP550	196, 686	0.179	516, 888	27.34
TSMN(CA)-Imp300	200	0.138	608, 1000	44.14
TSMN(CA)-Imp550	207	0.100	590	45.44
TSMN(CA)-SP300	202	0.235	471.47	43.74
TSMN(CA)-SP550	218, 670	0.099	573, 1000	46.69

polymolybdate (Mo_{36}) [41]. The intensity of this band is more pronounced for the catalysts synthesized with a complexing agent and calcined at 300 °C, indicating better dispersion of the active metals. These results are in agreement with those obtained with Raman spectroscopy and XRD.

3.1.6. Temperature-programmed desorption

The surface acidity characteristics of non-sulfided HDS catalysts were determined by NH_3-TPD. Ti, which is a tetravalent element, incorporates into the silica framework easily with improves surface acidity (see Fig. SI-3 and Table SI-1), and the nature of the acidity observed in all prepared catalysts is mostly weak and/or moderate, characterized by Lewis acid sites in the temperature range between 195° and 220 °C (Fig. 7 and Table 3) [42]. In all cases, the acidic strength of catalysts calcined at 300 °C is higher than the catalysts calcined at 550 °C. In addition, the catalysts prepared by the SP approach with or without citric acid [TSMN(CA)-SP300 and TSMN-SP300] have more surface acidity than the others. It seems that the incorporation of active metals at the beginning of catalyst preparation in the SP approach improves the acidity considerably. In addition, the surface acidity of Ti-modified SBA-15-NiMo HDS catalysts prepared by SP method at both calcination temperatures is higher than the unmodified SBA-15-NiMo catalysts prepared by the same approach (See Fig. SI-3 and Table SI-1).

3.1.7. Temperature-programmed reduction

The H_2-TPR profiles of catalysts prepared by the SP and impregnation approaches are shown in Fig. 8. A variation is noticed in the reduction temperature of the active metals (NiMo) due to either the active phase deposition method or calcination temperature. At relatively low temperature (410–560 °C), the main H_2 consumption temperature corresponding to the reduction of Mo polymeric octahedral (Mo^{6+} to Mo^{4+}) is observed, while the reduction temperature of H2 between (700–770 °C) could be attributed to (Mo^{4+} to Mo^0) of polymeric octahedral, tetrahedral and bulk molybdena species [25]. The reduction temperatures for the catalysts prepared at low calcination temperature (300 °C) are lower than those at high temperature (550 °C) in both cases of Mo reduction (Mo^{6+} to Mo^{4+} and Mo^{4+} to Mo^0) (Table 3). It has been reported that the increase in the reduction temperature is related to a strong metal support interaction, which decreases dispersion and in turn affects the catalytic performance. It is noteworthy that the use of citric acid (as a complexing agent) aids the dispersion of the active phase, as observed in the XRD and Raman spectroscopy results; this was further established by the lower reduction temperature in the H_2-TPR analysis. These results are in good agreement with the report by Badoga et al. [17], who used EDTA as a complexing agent.

3.1.8. Scanning electron microscopy

Images captured by scanning electron microscopy for non-sulfided HDS catalysts are presented in Fig. SI-4. For catalysts
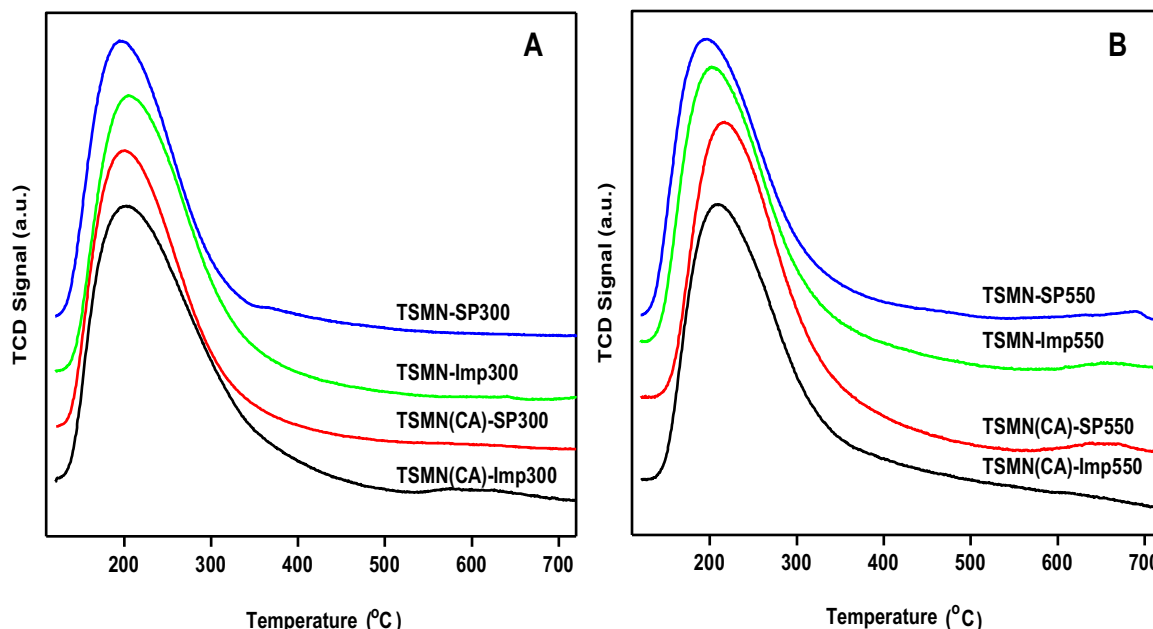
Fig. 7. NH$_3$-TPD Results of HDS Catalysts (in the Oxide Form) Calcined at (A) 300 °C and (B) 550 °C.
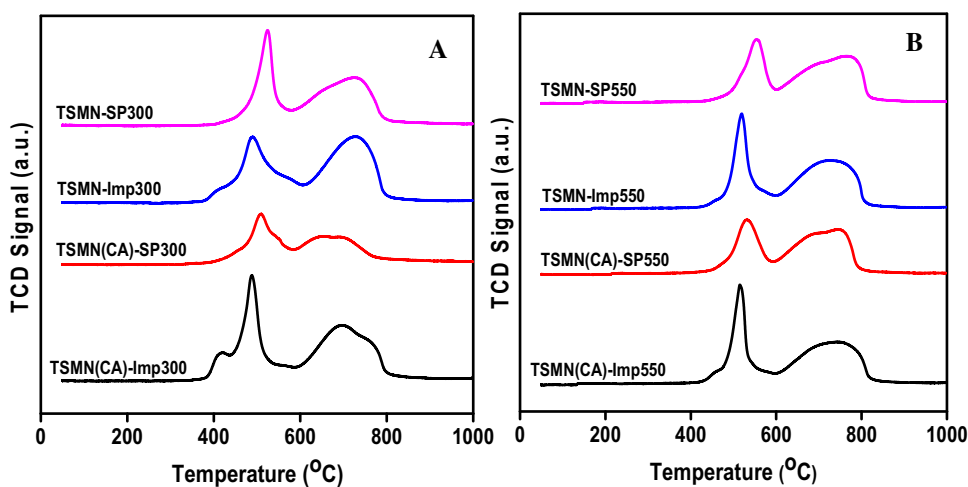

Fig. 8. H$_2$-TPR Results of HDS Catalysts (in the Oxide Form) Calcined at (A) 300 °C and (B) 550 °C.

prepared by the SP approach (with or without CA) subjected to a low calcination temperature (300 °C), a unique nano-cubical flat-sheet morphology of Mo is observed, and this morphology is grown alongside the rod-like morphology of heteroatom modified-SBA-15. However, the low calcination temperature catalysts obtained by the impregnation method show little or no NiMo particles on the surface of the support, which indicates that the active metals are preferably embedded in the SBA-15 structural unit. For all non-sulfided catalysts obtained at a high calcination temperature (550 °C), there are long rectangular rods of Mo on the support, which is responsible for the observed high-intensity crystalline phases of MoO$_3$. These results are in agreement with those obtained by Raman spectroscopy and XRD.

3.1.9. Transmission electron microscopy

Better understanding of active phase (MoS$_2$) distribution and dispersion of sulfided HDS catalysts, as a function of calcination temperature, addition of complexing agent and preparation method was obtained by HRTEM. The selected representative

micrographs (as shown in Fig. 9) showed the morphological and microstructural changes of NiMo supported on Ti-SBA-15 by impregnation and SP-approach. The arrows are pointed to the MoS$_2$ crystallites with measured interplanar distance of 0.61 nm. The crystallite lengths and stacking degrees are summarized in Table 4. The MoS$_2$ crystallite lengths of the catalyst prepared by impregnation approach without citric acid (TSMN-Imp300) is found between 2 and 4.4 nm, and the stacking degree of 1–2 layers, while the catalyst prepared by impregnation approach with citric acid exhibits slightly different MoS$_2$ crystallite lengths between 2 and 4.8 nm, and the same stacking layers with TSMN-Imp300. The crystallite lengths and stacking degree observed for TSMN(CA)-SP300 is similar to both catalysts prepared by impregnation approach at low calcination temperature. There is a slight variation in the distribution and morphology of TSMN-SP300 catalyst prepared by SP-approach at low calcination temperature, this catalyst exhibits longer MoS$_2$ crystallites between 2.5–5.0 nm, with layer stacking of 2–4 layers compared to other counterparts at low calcination temperature. On the other hand, the catalysts calcined at
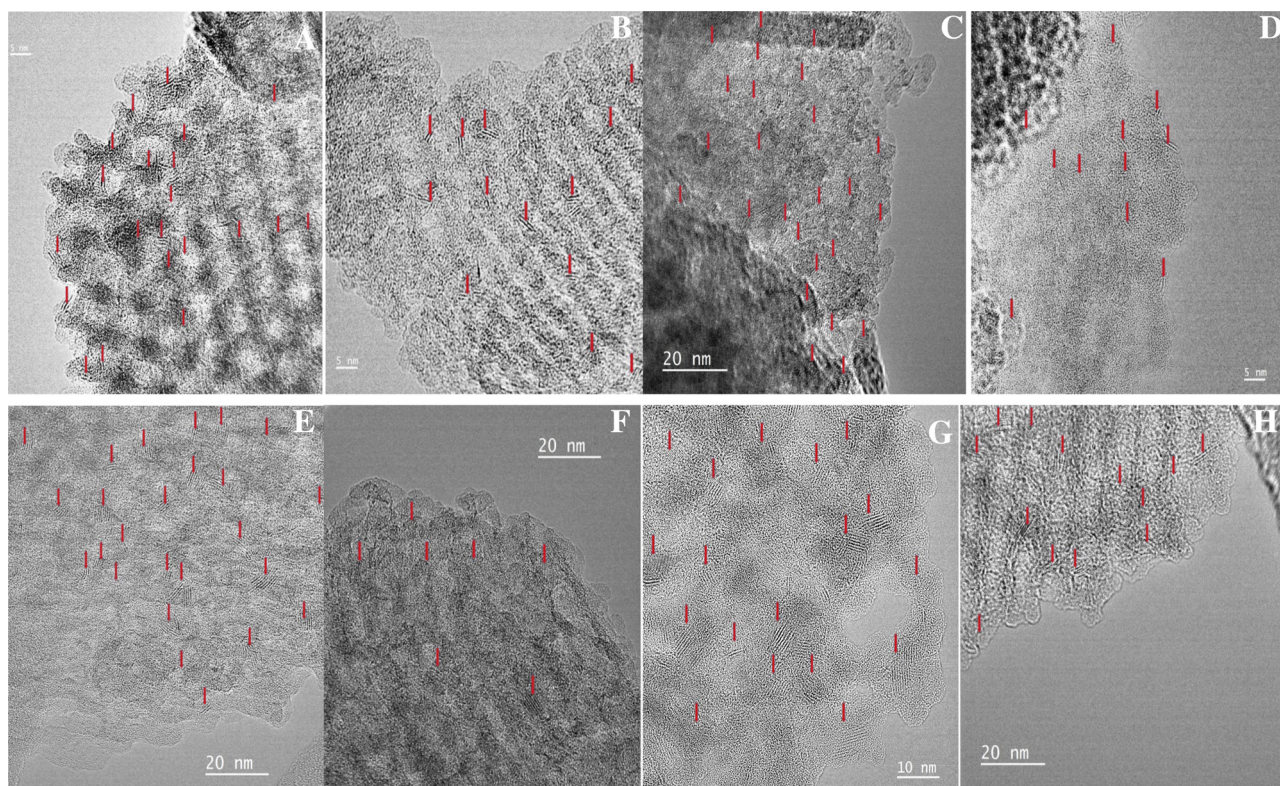
Fig. 9. HRTEM analysis of sulfided HDS catalysts (A) TSMN-Imp300, (B) TSMN(CA)-Imp300, (C) TSMN-SP300, (D) TSMN(CA)-SP300, (E) TSMN-Imp550, (F) TSMN(CA)-Imp550, (G) TSMN-SP550 and (H) TSMN(CA)-SP550.

Table 4
MoS$_2$ Crystallites Length and Stacking Degree Distribution.

Catalysts	Length Distribution (nm)	Average Length (nm)	Stacking Distribution (layers number)	Average stacking (layers number)
TSMN-Imp300	2–4.4	3.3	1–2	2.0
TSMN-Imp550	2–6.6	4.8	2–4	4.5
TSMN-SP300	2.5–5.0	3.8	2–4	3.1
TSMN-SP550	3–7.6	5.5	2–10	6.2
TSMN(CA)-Imp300	2–4.8	3.2	1–2	2.5
TSMN(CA)-Imp550	4–7.8	6.2	2–10	6.5
TSMN(CA)-SP300	2–4.4	3.3	1–2	2.5
TSMN(CA)-SP550	4–6.1	5.3	2–8	5.0

high temperature showed different active phase distributions and morphologies, with longer MoS$_2$ slab length and higher stacking degrees. As observed for non-sulfided oxide NiMo catalysts, the dispersion of low temperature catalysts is better than the corresponding high calcination temperature catalysts and thus expected to favor catalytic activities [43]. However, there is little distinction that can be deduced within the catalysts of the same group, with the exception of TSMN-Imp550 exhibiting better slab length and stacking degree than others at high calcination temperature.

3.1.10. X-ray photoelectron spectroscopy (XPS)

The surface composition and bonding state of representative sulfided HDS catalysts were analyzed by XPS. The spectra for Mo and S states are presented in (Fig. 10A and B), respectively and the atomic weight of all elements are summarized in (Table SI-2). Being a surface analysis technique, the distribution and degree of sulfidation can be explained to some extent. As observed from Mo spectra, all catalysts possessed significant amount of Mo^{6+} (d$_{5/2}$) oxidation state between 232 and 232.8 eV, while the bonding state of molybdenum corresponding to Mo^{4+} (as in MoS$_2$) is observed between 229 and 229.8 eV. In addition, we observed contribution

of sulfur around 226.6 eV, corresponding to 2S line, and this is subtracted from molybdenum composition [44]. As shown in Fig. 10B, the XPS peak attributed to sulfide in MoS$_2$ form is between 161 and 163.8, which is present for all catalysts in different degrees. In addition to MoS$_2$ peak, a peak corresponding to oxy-sulfide is present (168–170 eV). We observed from atomic weight percent calculation (Table SI-2) different degree of sulfidation among the HDS catalysts, with the highest for TSMN-Imp300 and the lowest for TSMN-SP550. This result confirms that the low calcination temperature catalysts are relatively more dispersed than high calcination temperature counterparts.

3.1.11. Chemical compositions of HDS catalysts

The chemical compositions of bulk catalysts prepared both SP and impregnation approach was investigated by ICP-OES analysis. It is observed that main active element (molybdenum) is well attached to the support (Ti-SBA-15) by both deposition methods, and all the catalysts possessed reasonable amount of the ca. 13 wt.%. However, there is a disparity in the amount of nickel observed in both active phase deposition approaches. In the case of impregnation approach, nickel is well attached to the support irrespective of
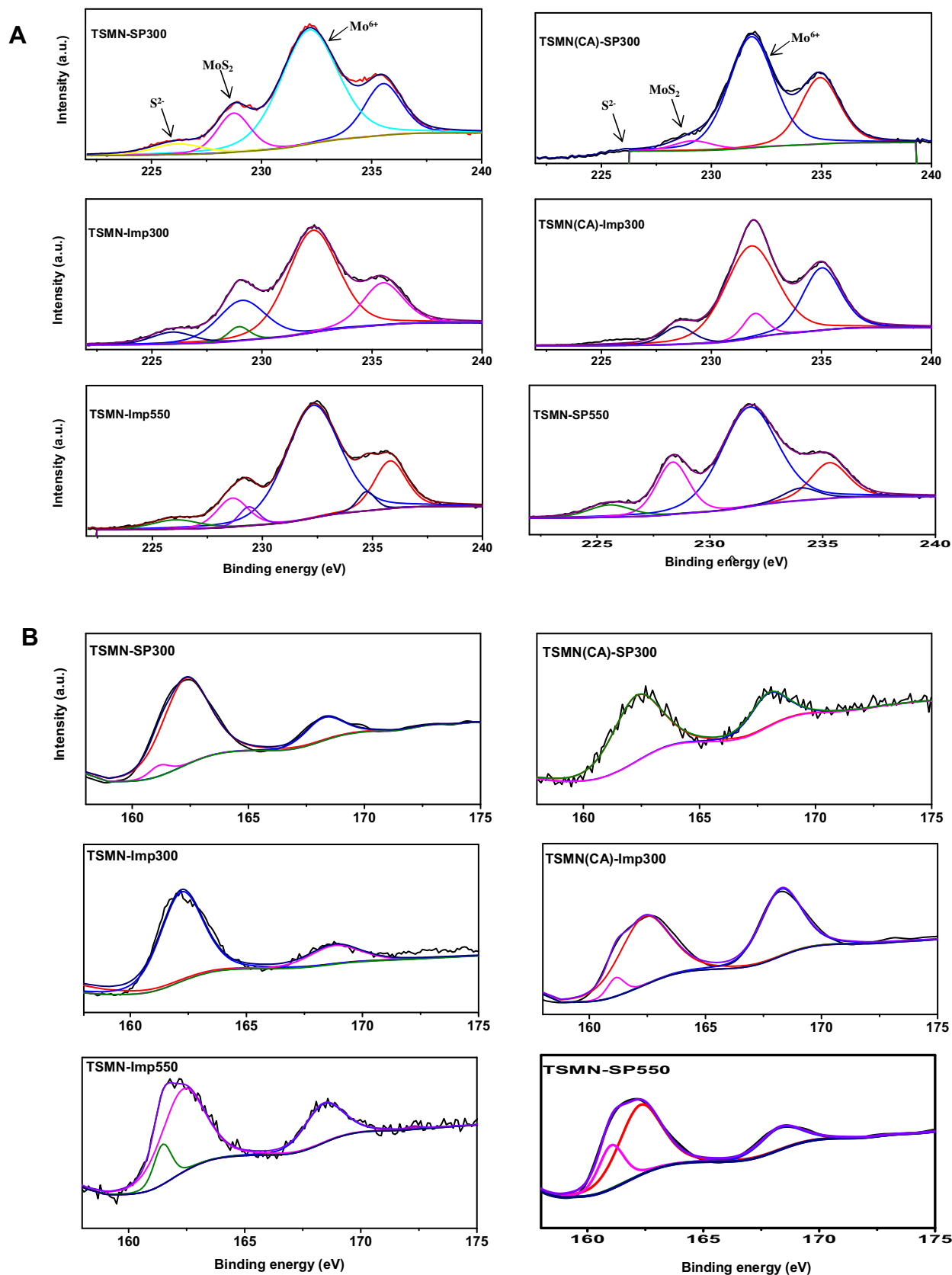
Fig. 10. A X-Aray Photoelectron Spectroscopy Analysis of Sulfided HDS Catalysts Showing Molybdenum Bonding States. B X-Bray Photoelectron Spectroscopy Analysis of Sulfided HDS Catalysts Showing Molybdenum Bonding States.
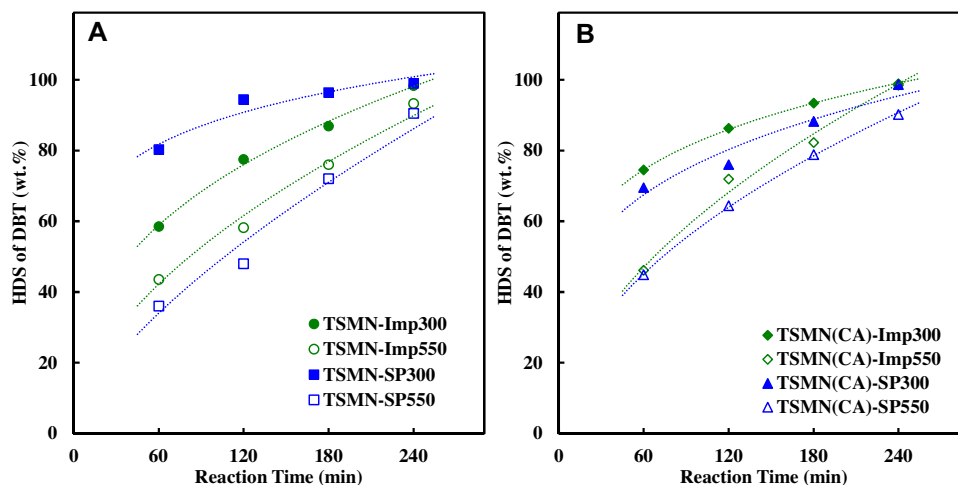
Fig. 11. Activities of Synthesized Catalysts for the HDS of DBT at Different Contact Times.

Table 5
Elemental Composition by ICP-OES.

Catalysts	Elements		
	Mo (%)	Ni (%)	Si/Ti
TSMN-Imp300	12.90	2.95	9.98
TSMN-Imp550	13.18	3.02	9.92
TSMN-SP300	12.46	1.63	10.04
TSMN-SP550	12.98	1.84	10.15
TSMN(CA)-Imp300	13.01	2.96	9.97
TSMN(CA)-Imp550	11.18	2.99	10.01
TSMN(CA)-SP300	11.92	1.39	10.12
TSMN(CA)-SP550	13.31	1.26	10.26

Table 6
Catalyst Performance Test Results: Product Sulfur Content. (Process Conditions: 350 °C; 5 MPa; Reaction Time: 4 h; Feed Sulfur Content = 2500 ppm).

Catalysts	Product Sulfur Content (ppm)			
	1 h	2 h	3 h	4 h
TSMN-Imp300	1038	562	327	41
TSMN-Imp550	1411	1046	600	168
TSMN-SP300	494	139	90	25
TSMN-SP550	1600	1300	700	238
TSMN(CA)-Imp300	639	343	164	27
TSMN(CA)-Imp550	1349	702	443	37
TSMN(CA)-SP300	763	600	295	34
TSMN(CA)-SP550	1377	889	529	247

the calcination temperature, while the SP-approach suffers significant loss in the amount of nickel present in the final HDS catalysts (Table 5). This disparity could be due to the presence of soluble nickel in the solution that could be not completely anchored to the support under synthesis parameters and method [45].

3.2. HDS activities of synthesized catalysts

The sulfur contents of the products at different reaction times are presented in Table 6. The results show a significant variation in the performance of the synthesized catalysts, which indicates the influence of the preparation method (SP versus impregnation), calcination temperature (300 °C versus 550 °C), and complexing agent. In terms of initial activity, which can be estimated by the product sulfur content after one hour, catalysts calcined at 300 °C perform better than those calcined at 500 °C, irrespective of the preparation method or the use of a complexing agent. When the complexing agent is not used, the performance of the catalyst pre-
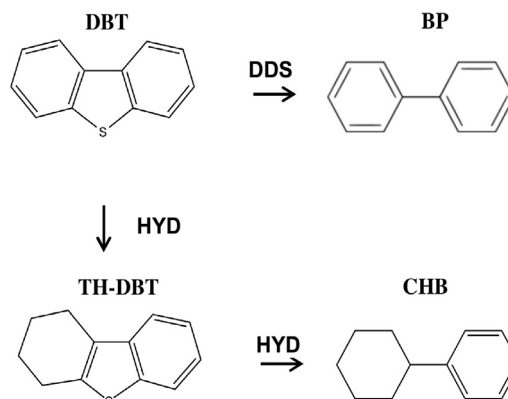

Fig. 12. Reaction Pathways for the HDS of DBT.

pared by the SP method (TSMN-SP300) is significantly better than the catalyst prepared by the conventional impregnation method (TSMN-Imp 300). The trend of the initial activity is observed to be TSMN-SP300 > TSMN-Imp300 > TSMN-Imp550 > TSMNSP550. This trend continues with increased reaction time, as shown in Fig. 11A.

For the catalysts prepared using the complexing agent, the influence of the preparation method (SP versus impregnation) is modest, but impregnation is better. However, the influence of calcination temperature remains significant. Thus, the trend in the initial activity is found to be TSMN(CA)-Imp300 > TSMN(CA)-SP300 > TSMN(CA)-Imp550 ~ TSMN(CA)-SP550. With the increase in reaction time, however, the influence of calcination temperature also diminishes, as shown in Fig. 11B.

In addition, the significant effect of citric acid at the end of reaction time (4 h) is noticeable as shown in Table 6, especially for the catalyst prepared by impregnation approach. It is observed that the catalyst prepared by impregnation approach with CA at low and high calcination temperatures, showed higher activity of sulfur removal by (98.92% against 98.36%) and (98.52% against 93.28%), respectively, than without CA.

3.2.1. Reaction pathways

The HDS of DBT occurs via two parallel pathways as illustrated in Fig. 12: (i) direct desulfurization (DDS) or hydrogenolysis by C—S bond cleavage in a single step; or (ii) hydrogenation (HYD) in 2–3 steps through the hydrogenation of one of the phenyl rings followed by C—S bond cleavage [46]. The HDS of DBT via the DDS pathway

Table 7

Catalyst Performance Test Results: Product Distribution. (Process Conditions: 350 °C; 5 MPa; Reaction Time: 1 h).

Catalysts	Product Distribution (wt.%)			BP/CHB
	CHB	BP	4HDBT	
TSMN-Imp300	19.91	80.09	–	4.02
TSMN-Imp550	31.61	61.72	6.67	1.95
TSMN-SP300	9.12	90.89	–	9.97
TSMN-SP550	14.63	76.42	8.95	5.22
TSMN(CA)-Imp300	32.13	67.87	–	2.11
TSMN(CA)-Imp550	28.52	71.48	–	2.51
TSMN(CA)-SP300	14.70	85.30	–	5.80
TSMN(CA)-SP550	14.94	76.49	8.57	5.12

yields biphenyl (BP) and H_2S as final products. However, the HYD pathway results in the formation of intermediates, such as tetrahydro dibenzothiophene (THDBT) and hexahydro dibenzothiophene (HHDBT), followed by fast desulfurization to form cyclohexyl benzene (CHB). Because the DDS pathway consumes substantially less hydrogen, it is the preferred route.

The analysis of hydrocarbon products obtained after one hour of reaction time over different synthesized catalysts is presented in Table 7. BP is the predominant compound in all products, indicating that DDS is the generally preferred route. However, there are significant differences in the preference for DDS among the synthesized catalysts as revealed by the BP/CHB ratio in the products. When a complexing agent is not used, the catalysts calcined at 300 °C exhibit approximately twice the BP/CHB ratio of catalysts calcined at 550 °C. The catalysts prepared by the SP method and calcined at 300 °C show exceptional preference for the DDS route with a BP/CHB ratio of approximately 10. The use of a complexing agent significantly reduces the BP/CHB ratio, which indicates that the direct scission of the C-S bond is not effective and that the hydrogenation reaction is also enhanced. The effect of calcination temperature on the BP/CHB ratio is not significant when complexing is used.

The 4-HDBT intermediate is detected only in products obtained from TSMN-Imp550, TSMN-SP550, and TSMN(CA)-SP550. These are low-activity catalysts, which also result in higher sulfur contents (>150 ppm) in the products even after a contact time of 4 h (Table 6).

3.2.2. HDS kinetics

The HDS rates were calculated assuming pseudo-first order kinetics, and the values of the reaction constant, k (min^{-1}), were determined using the initial conversion values – those obtained after the first hour of the reaction. The results presented in Table 8 show that the value of the HDS rate constant is 13.5×10^{-3} min^{-1} for the TSMN-Imp300 catalyst. This value compares well with the reported rate constant of 18.3×10^{-3} min^{-1} for the HDS of DBT at 350 °C over a CoMo/Al$_2$O$_3$ catalyst [44].

3.2.2.1. Effect of calcination temperature.
The decrease in the calcination temperature from 550 °C to 300 °C results in consistently

higher HDS rates. The catalyst prepared by the impregnation method without the complexing agent (TSMN-Imp550) exhibits an HDS rate of 8.4×10^{-3} min^{-1}, which is increased by approximately 61% to 13.5×10^{-3} min^{-1} when the calcination temperature is reduced (TSMN-Imp300). The catalyst prepared by the SP method and calcined at 300 °C (TSMN-SP300) exhibits the highest rate constant of 25.6×10^{-3} min^{-1}, which is approximately four times the rate obtained with TSMN-SP550. The trend of a higher HDS rate for the catalysts calcined at 300 °C is also observed for the catalysts prepared using a complexing agent. However, the increase is moderately higher for the catalysts prepared by the impregnation method (47%) compared with those prepared by the SP method (41%). It seems that the addition of a complexing agent offsets some of the benefits of a lower calcination temperature.

The rate constants for the DDS and HYD pathways are presented in Table 8 as k_{DDS} and k_{HYD}, respectively. In addition to the significant increase in the HDS rates, a lower calcination temperature is effective in promoting HDS by the DDS pathway. The catalyst prepared by the impregnation method without the complexing agent (TSMN-Imp550) exhibits a k_{DDS}/k_{HYD} ratio of 1.7, which is increased by three times when the calcination temperature is reduced (TSMN-Imp300). The catalyst prepared by the SP method and calcined at 300 °C (TSMN-SP300) exhibits the highest k_{DDS}/k_{HYD} ratio of 17.2, which is approximately five times the rate obtained with TSMN-SP550. It should be noted that while k_{DDS} increases four times due to a reduction in the calcination temperature, k_{HYD} remains unchanged. This observation indicates that the active sites for DDS may be different from those in the HYD pathway.

The trend of a higher HDS rate for the catalysts calcined at 300 °C is also observed for the catalysts prepared by the SP method using a complexing agent. However, the increase is not as drastic as that observed with the catalysts prepared without the complexing agent.

As shown in Section 3.1, the catalyst prepared by the SP method and calcined at 300 °C (TSMN-SP300) possesses a significantly higher surface area (460 m^2/g) and pore volume (0.66 cm^3/g) compared to the catalyst calcined at 550 °C (TSMN-SP550). This method provides a much better dispersion of active metals and better accessibility to reactants. TSMN-SP300 also exhibits the highest surface acidity among the catalysts prepared without the addition of a complexing agent. XRD results also show that the catalysts calcined at 300 °C exhibit better dispersion of active metals on the support and the presence of small crystallites. Similar trends are observed by Raman spectroscopy and FTIR spectroscopy. HRTEM results presented in Fig. 9 and Table 4 show shorter MoS$_2$ crystallite length as well as lower stacking distributions for TSMN-SP300 compared to TSMN-SP550, which indicate a significant effect of calcination temperature on the catalyst morphology. Lower calcination temperature (300 °C) clearly resulted in better dispersion of molybdenum sulfide phase. Hence highest overall HDS rate of TSMN-SP300 as well as the increased DDS activity can be attributed to better dispersion of molybdenum, higher acidity and more accessible pore structure.

Table 8

First-Order Rate Constants for HDS of DBT at 350 °C.

Catalysts	$k_{HDS} \times 10^3$ (min^{-1})	$k_{DDS} \times 10^3$ (min^{-1})	$k_{HYD} \times 10^3$ (min^{-1})	k_{DDS}/k_{HYD}
TSMN-Imp300	13.6	10.5	2.1	5.1
TSMN-Imp550	8.4	5.2	3.0	1.7
TSMN-SP300	25.6	21.8	1.4	17.2
TSMN-SP550	6.5	5.4	1.5	3.6
TSMN(CA)-Imp300	19.7	11.7	4.6	2.6
TSMN(CA)-Imp550	10.4	6.7	2.4	2.8
TSMN(CA)-SP300	15.8	15.0	1.8	8.3
TSMN(CA)-SP550	9.3	7.0	1.9	3.8

3.2.2.2. Effect of preparation method. Comparison of the HDS rates exhibited by catalysts prepared by the two methods investigated in this study, i.e., impregnation and SP, provides insight into the efficacy of each method. The SP approach presents new, simple, and easy steps in catalyst design and preparation, which leads to low-cost catalyst design and the incorporation of the active phase within the mesoporous framework. The catalyst prepared by the SP method exhibits higher HDS activity compared to catalyst prepared by impregnation when the calcination temperature is 300 °C. The overall HDS rate constant of TSMN-SP300 is approximately 90% higher than the rate constant of TSMN-Imp300. Moreover, HDS by DDS is significantly enhanced by TSMN-SP300, resulting in a 3.5-fold increase in the k_{DDS}/k_{HYD} ratio. However, when the calcination temperature is increased to 550 °C, the catalyst prepared by the SP method exhibits lower activity, and the benefits of the SP method in terms of the k_{DDS}/k_{HYD} ratio are drastically reduced.

HRTEM results indicate insignificant differences between the catalysts prepared by the SP and impregnation methods at corresponding calcination temperatures in terms of MoS_2 crystallites length and stacking distribution. Hence, the dispersion of molybdenum sulfide does not seems to be effected by the preparation method. However, the main differences in the characteristics of the catalysts prepared by the SP and impregnation methods are the significantly higher surface area (especially the external surface area) and pore volume for SP catalysts. The catalysts prepared by the SP method also possess higher surface acidity, which can enhance C-S bond scission and result in higher DDS.

The use of a complexing agent improves the performance of catalysts prepared by the impregnation method. The increase in the HDS rate from TSMN-Imp 300 to TSMN(CA)-Imp300 is 46%. However, this improvement is reduced to only 24% when the calcination temperature is increased to 550 °C. The use of a complexing agent affected the performance of catalysts prepared by the SP method in a different manner. Although the complexing agent is beneficial for the overall HDS rate when the calcination temperature is 550 °C, it exhibits a negative impact at the calcination temperature of 300 °C. However, the k_{DDS}/k_{HYD} ratio of 8.3 for TSMN(CA)-SP300 is the highest among all catalysts prepared using a complexing agent.

The incorporation of a complexing agent improves the dispersion of active metals as observed by XRD and Raman spectroscopy. The impact of better dispersion is evident from the improved HDS activity of catalysts prepared by the impregnation method, i.e., by comparing TSMN(CA)-Imp300 and TSMN(CA)-Imp550 to TSMN-Imp300 and TSMN-Imp550, respectively. However, the catalysts prepared by the SP method are negatively affected by the complexing agent.

In general, the HDS activities of the SP-approach catalysts at a low calcination temperature are better than the other catalysts within the series, and it is noteworthy that better performance could be achieved without the use of a complexing agent to aid the dispersion of active metals. Therefore, the preparation of supported HDS catalysts at a low calcination temperature leads to deep desulfurization within a short period of time could be attributed to high dispersion of the active phase, as indicated by the Raman spectroscopy, XRD analyses and HRTEM results.

4. Conclusions

The single-pot (SP) synthesis of NiMo-supported Ti-SBA-15 HDS catalyst was successfully developed, and the catalyst was evaluated for the HDS of dibenzothiophene. The results with this catalyst were compared with those using the established impregnation approach. The catalyst from the SP approach exhibited a great potential to minimize the time involved in catalyst design and preparation. Furthermore, the use of a complexing agent to improve dispersion

and prevent the formation of crystalline $NiMoO_4$ was unnecessary. Overall, the SP catalyst formed at a low calcination temperature (TSMN-SP300) possessed superior catalytic performance and selectivity for direct desulfurization compared with the other studied catalysts. The dispersion, surface acidity, and textural properties were contributing factors that improved catalytic efficiency.

Appendix A. Supplementary data

Supplementary data associated with this article can be found, in the online version, at http://dx.doi.org/10.1016/j.apcatb.2016.10.052.

References

[1] C. Song, An overview of new approaches to deep desulfurization for ultra-clean gasoline, diesel fuel and jet fuel, Catal. Today 86 (2003) 211–263.
[2] C. Song, Fuel processing for low-temperature and high-temperature fuel cells: challenges, and opportunities for sustainable development in the 21 st century, Catal. Today 77 (2002) 17–49.
[3] L. Qu, W. Zhang, P.J. Kooyman, R. Prins, MAS NMR, TPR, and TEM studies of the interaction of NiMo with alumina and silica-alumina supports, J. Catal. 215 (2003) 7–13.
[4] V. Sundaramurthy, I. Eswaramoorthi, A. Dalai, J. Adjaye, Hydrotreating of gas oil on SBA-15 supported NiMo catalysts, Microporous Mesoporous Mater. 111 (2008) 560–568.
[5] T. Klimova, L. Pena, L. Lizama, C. Salcedo, O.Y. Gutiérrez, Modification of activity and selectivity of NiMo/SBA-15 HDS catalysts by grafting of different metal oxides on the support surface, Ind. Eng. Chem. Res. 48 (2008) 1126–1133.
[6] J. Duchet, M. Tilliette, D. Cornet, L. Vivier, G. Perot, L. Bekakra, C. Moreau, G. Szabo, Catalytic properties of nickel molybdenum sulphide supported on zirconia, Catal. Today 10 (1991) 579–592.
[7] G.M. Kumaran, S. Garg, K. Soni, V. Prasad, L. Sharma, G.M. Dhar, Catalytic functionalities of H-β-zeolite-supported molybdenum hydrotreating catalysts, Energy Fuels 20 (2006) 1784–1790.
[8] M. Breysse, P. Afanasiev, C. Geantet, M. Vrinat, Overview of support effects in hydrotreating catalysts, Catal. Today 86 (2003) 5–16.
[9] N. Prabhu, A. Dalai, J. Adjaye, Hydrodesulphurization and hydrodenitrogenation of light gas oil using NiMo catalyst supported on functionalized mesoporous carbon, Appl. Catal. A: Gen. 401 (2011) 1–11.
[10] V. Meynen, P. Cool, E. Vansant, Synthesis of siliceous materials with micro-and mesoporosity, Microporous Mesoporous Mater. 104 (2007) 26–38.
[11] S. Badoga, K.C. Mouli, K.K. Soni, A. Dalai, J. Adjaye, Beneficial influence of EDTA on the structure and catalytic properties of sulfided NiMo/SBA-15 catalysts for hydrotreating of light gas oil, Appl. Catal. B: Environ. 125 (2012) 67–84.
[12] N. Rinaldi, T. Kubota, Y. Okamoto, Effect of citric acid addition on Co-Mo/B2O3/Al2O3 catalysts prepared by a post-treatment method, Ind. Eng. Chem. Res. 48 (2009) 10414–10424.
[13] G. Kishan, L. Coulier, V. De Beer, J. Van Veen, J. Niemantsverdriet, Sulfidation and thiophene hydrodesulfurization activity of nickel tungsten sulfide model catalysts, prepared without and with chelating agents, J. Catal. 196 (2000) 180–189.
[14] M.S. Rana, J. Ramírez, A. Gutiérrez-Alejandre, J. Ancheyta, L. Cedeño, S. Maity, Support effects in CoMo hydrodesulfurization catalysts prepared with EDTA as a chelating agent, J. Catal. 246 (2007) 100–108.
[15] M. Lélias, E. Le Guludec, L. Mariey, J. Van Gestel, A. Travert, L. Oliviero, F. Maugé, Effect of EDTA addition on the structure and activity of the active phase of cobalt–molybdenum sulfide hydrotreatment catalysts, Catal. Today 150 (2010) 179–185.
[16] R. Huirache-Acuña, R. Nava, C.L. Peza-Ledesma, J. Lara-Romero, G. Alonso-Núez, B. Pawelec, E.M. Rivera-Muñoz, SBA-15 mesoporous silica as catalytic support for hydrodesulfurization catalysts—review, Materials 6 (2013) 4139–4167.
[17] S. Badoga, A.K. Dalai, J. Adjaye, Y. Hu, Combined effects of EDTA and heteroatoms (Ti, Zr, and Al) on catalytic activity of SBA-15 supported NiMo catalyst for hydrotreating of heavy gas oil, Ind. Eng. Chem. Res. 53 (2014) 2137–2156.

[18] L. Pena, D. Valencia, T. Klimova, CoMo/SBA-15 catalysts prepared with EDTA and citric acid and their performance in hydrodesulfurization of dibenzothiophene, Appl. Catal. B: Environ. 147 (2014) 879–887.

[19] D. Valencia, T. Klimova, Citric acid loading for MoS 2-based catalysts supported on SBA-15. New catalytic materials with high hydrogenolysis ability in hydrodesulfurization, Appl. Catal. B: Environ. 129 (2013) 137–145.

[20] O.Y. Gutiérrez, S. Singh, E. Schachtl, J. Kim, E. Kondratieva, J. Hein, J.A. Lercher, Effects of the support on the performance and promotion of (Ni) MoS2 catalysts for simultaneous hydrodenitrogenation and hydrodesulfurization, ACS Catal. 4 (2014) 1487–1499.

[21] Z. Liu, L. Zhang, J. Jiang, C. Bian, Z. Zhang, Z. Gao, Advancement of hydro-desulfurization catalyst and discussion of its application in coal tar, Adv. Chem. Eng. Sci. 3 (2013) 36–46.

[22] P.-Y. Wu, S.-F. Ji, L.-H. Hu, J.-Q. Zhu, C.-Y. Li, Preparation, characterization, and catalytic properties of the Mo2C/SBA-15 catalysts, J. Porous Mater. 15 (2008) 181–187.

[23] P. Castaño, B. Pawelec, J. Fierro, J. Arandes, J. Bilbao, Enhancement of pyrolysis gasoline hydrogenation over Pd-promoted Ni/SiO2-Al2O3 catalysts, Fuel 86 (2007) 2262–2274.

[24] D. Zhao, J. Feng, Q. Huo, N. Melosh, G.H. Fredrickson, B.F. Chmelka, G.D. Stucky, Triblock copolymer syntheses of mesoporous silica with periodic 50 to 300 angstrom pores, Science 279 (1998) 548–552.

[25] M.Á. Calderón-Magdaleno, J.A. Mendoza-Nieto, T.E. Klimova, Effect of the amount of citric acid used in the preparation of NiMo/SBA-15 catalysts on their performance in HDS of dibenzothiophene-type compounds, Catal. Today 220 (2014) 78–88.

[26] K. Cassiers, T. Linssen, M. Mathieu, M. Benjelloun, K. Schrijnemakers, P. Van Der Voort, P. Cool, E. Vansant, A detailed study of thermal, hydrothermal, and mechanical stabilities of a wide range of surfactant assembled mesoporous silicas, Chem. Mater. 14 (2002) 2317–2324.

[27] Z. Jin, X. Wang, X. Cui, Synthesis and morphological investigation of ordered SBA-15-type mesoporous silica with an amphiphilic triblock copolymer template under various conditions, Coll. Surf. A: Physicochem. Eng. Aspects 316 (2008) 27–36.

[28] S. Badoga, R.V. Sharma, A.K. Dalai, J. Adjaye, Hydrotreating of heavy gas oil on mesoporous zirconia supported NiMo catalyst with EDTA, Fuel 128 (2014) 30–38.

[29] H. Sun, C. Wang, S. Pang, X. Li, Y. Tao, H. Tang, M. Liu, Photocatalytic TiO2 films prepared by chemical vapor deposition at atmosphere pressure, J. Non-Cryst. Solids 354 (2008) 1440–1443.

[30] O.Y. Gutiérrez, F. Pérez, G.A. Fuentes, X. Bokhimi, T. Klimova, Deep HDS over niMo/Zr-SBA-15 catalysts with varying MoO 3 loading, Catal. Today 130 (2008) 292–301.

[31] W. Li, G.D. Meitzner, R.W. Borry, E. Iglesia, Raman and X-ray absorption studies of Mo species in Mo/H-ZSM5 catalysts for non-oxidative CH4 reactions, J. Catal. 191 (2000) 373–383.

[32] Y.V. Plyuto, I. Babich, I. Plyuto, A. Van Langeveld, J. Moulijn, Synthesis and characterization of molybdenum (VI) oxo-species on the surface of fumed alumina and silica, Coll. Surf. A: Physicochem. Eng. Aspects 125 (1997) 225–230.

[33] G. Mestl, P. Ruiz, B. Delmon, H. Knozinger, Oxygen-exchange properties of MoO3: an in situ Raman spectroscopy study, J. Phys. Chem. 98 (1994) 11269–11275.

[34] B.C. Windom, W. Sawyer, D.W. Hahn, A Raman spectroscopic study of MoS2 and MoO3: applications to tribological systems, Tribol. Lett. 42 (2011) 301–310.

[35] M. Py, P.E. Schmid, J. Vallin, Raman scattering and structural properties of MoO3, Il Nuovo Cimento B (1971–1996) 38 (1977) 271–279.

[36] M. Dieterle, G. Weinberg, G. Mestl, Raman spectroscopy of molybdenum oxides Part I. Structural characterization of oxygen defects in MoO3-x by DR UV/VIS, Raman spectroscopy and X-ray diffraction, Phys. Chem. Chem. Phys. 4 (2002) 812–821.

[37] K. Amakawa, P. Hildebrandt, R. Schlögl, R. Schomäcker, C. Limberg, Active Site for Propene Metathesis in Silica-supported Molybdenum Oxide Catalysts, Technische Universität Berlin, 2013.

[38] S. Braun, L.G. Appel, V.L. Camorim, M. Schmal, Thermal spreading of MoO3 onto silica supports, J. Phys. Chem. B 104 (2000) 6584–6590.

[39] S. Maity, M. Rana, S. Bej, J. Ancheyta-Juarez, G.M. Dhar, T.P. Rao, Studies on physico-chemical characterization and catalysis on high surface area titania supported molybdenum hydrotreating catalysts, Appl. Catal. A: Gen. 205 (2001) 215–225.

[40] L.Y. Lizama, T.E. Klimova, SBA-15 modified with Al Ti, or Zr as supports for highly active NiW catalysts for HDS, J. Mater. Sci. 44 (2009) 6617–6628.

[41] Z. Han, W. Pei, J. Xie, Y. Zou, X.-M. Ren, Two {Mo 36}-containing polymolybdates: synthesis, crystal structures, and spectral characterizations, Inorg. Chem. Commun. 16 (2012) 61–64.

[42] A. Tuel, Modification of mesoporous silicas by incorporation of heteroelements in the framework, Microporous Mesoporous Mater. 27 (1999) 151–169.

[43] O.Y. Gutiérrez, G.A. Fuentes, C. Salcedo, T. Klimova, SBA-15 supports modified by Ti and Zr grafting for NiMo hydrodesulfurization catalysts, Catal. Today 116 (2006) 485–497.

[44] W. Lai, Z. Chen, J. Zhu, L. Yang, J. Zheng, X. Yi, W. Fang, A NiMoS flower-like structure with self-assembled nanosheets as high-performance hydrodesulfurization catalysts, Nanoscale 8 (2016) 3823–3833.

[45] Y. Li, D. Pan, C. Yu, Y. Fan, X. Bao, Synthesis and hydrodesulfurization properties of NiW catalyst supported on high-aluminum-content, highly ordered, and hydrothermally stable Al-SBA-15, J. Catal. 286 (2012) 124–136.

[46] S.A. Ali, S. Ahmed, K.W. Ahmed, M.A. Al-Saleh, Simultaneous hydrodesulfurization of dibenzothiophene and substituted dibenzothiophenes over phosphorus modified CoMo/Al2O3 catalysts, Fuel Process. Technol. 98 (2012) 39–44.